

Effect of Accelerated Fe-Rich Precipitation Induced by Ag Addition on the Microstructure and Comprehensive Properties of Cu–10 Wt Pct Fe Alloys



JUNQI SHI, LUN ZHAO, LIANGGUO CHEN, SHUNRAN ZHANG, ZHONGZE LIN, GANPEI TANG, LANG REN, PEIJIAN SHI, TIANXIANG ZHENG, YIFENG GUO, QIANG LI, ZHE SHEN, BIAO DING, and YUNBO ZHONG

In this study, the effect of accelerated Fe-rich precipitation caused by Ag addition on the refinement of solidified microstructure and the improvement of electrical, mechanical, and magnetic properties of Cu–10Fe alloys was systematically investigated. Firstly, the quadruple refinement of Cu grains, micron-sized primary Fe-rich spheres and dendrites, and nano-sized Fe-rich precipitates in as-cast Cu–10Fe alloys was induced by the accelerated Fe-rich precipitation. Secondly, the saturation magnetization of as-cast Cu–10Fe alloys was improved, which is mainly dominated by the accelerated precipitation of micron-sized Fe-rich spheres and dendrites, rather than that of nano-sized Fe-rich precipitates. Moreover, the yield strength of cold-rolled Cu–10Fe alloys was increased, which can be attributed to the accelerated precipitation of nano-sized Fe-rich phases and their pinning effect on dislocation movement during cold-rolling. In the end, the synergistic enhancement of strength, ductility, and electrical conductivity of aged Cu–10Fe alloys was obtained by Ag addition, which guides the preparation of high-performance Cu–Fe alloys.

<https://doi.org/10.1007/s11661-022-06927-4>

© The Minerals, Metals & Materials Society and ASM International 2022

I. INTRODUCTION

Cu alloys are widely used in high-speed rail transit, electronic communications, aerospace, and other fields because they combine high strength and electrical conductivity.^[1–3] The further subdivision of modern industry puts forward higher requirements on various properties of Cu alloys.^[4,5] For example, with the gradual popularization of 5G technology, the substantial increase in communication frequency requires the Cu alloys used for electronic equipment with high strength and high thermal conductivity, as well as high electromagnetic shielding performance.^[6,7] Cu–Fe alloys

are considered one of the candidate materials. For Cu–Fe alloys, thermal conductivity and electromagnetic shielding properties are closely related to the electrical conductivity and magnetic properties, respectively.^[8,9] Therefore, how to simultaneously improve the strength, electrical conductivity, and magnetic properties has become the research focus of Cu–Fe alloys.^[10–12]

Refined nanoscale microstructure and accumulated abundant dislocations can be obtained through severe plastic deformation to improve the strength of Cu–Fe alloy, such as heavy cold drawing and high-pressure torsion.^[13,14] But the Cu–Fe alloys prepared by this method not only have poor thermal stability but also have low electrical conductivity.^[15] Microalloying methods have been widely studied to improve the comprehensive properties of Cu alloys.^[16,17] The mechanical properties of Cu–Fe alloys can effectively be improved by the addition of Cr,^[18] Si,^[19,20] and Nb^[21] while at the expense of electrical conductivity. The added Ag can simultaneously improve the strength and electrical conductivity of Cu–Fe alloys, which has attracted much attention.^[22,23] Xie *et al.*^[24] suggested that the interfacial energy between Cu and Fe can be reduced by the added Ag, which will reduce the critical nucleation radius of Fe nuclei, thereby refining the primary Fe-rich phases. Wang *et al.*^[25] used first-principles calculations to study

JUNQI SHI, LUN ZHAO, LIANGGUO CHEN, SHUNRAN ZHANG, ZHONGZE LIN, GANPEI TANG, LANG REN, PEIJIAN SHI, TIANXIANG ZHENG, YIFENG GUO, QIANG LI, ZHE SHEN, BIAO DING, and YUNBO ZHONG are with the State Key Laboratory of Advanced Special Steel & Shanghai Key Laboratory of Advanced Ferrometallurgy & School of Materials Science and Engineering, Shanghai University, 333 Nanchen Road, Shanghai 200444, P.R. China. Contact e-mails: zhshen@shu.edu.cn; dingbiao312@shu.edu.cn; yunboz@shu.edu.cn

Manuscript submitted July 11, 2022; accepted December 1, 2022.

Article published online December 20, 2022

the effect of added Ag on the diffusion activation energy of Fe in Cu–Fe alloys and then proposed an accelerated precipitation mechanism of micron-sized Fe-rich dendrites induced by Ag addition. The stress concentration during the tensile process can be weakened by the refinement of primary Fe-rich phases, thereby improving the mechanical properties of Cu–Fe alloys. Yuan *et al.*^[26] found that the added Ag can also reduce the solid solution of Fe in the Cu matrix and accelerate the precipitation of nano-sized Fe-rich phases and then obtain the synergistic improvement in strength and electrical conductivity of Cu–Fe alloys.

At present, the research on Cu–Fe–Ag alloy mainly focuses on the accelerated precipitation of Fe-rich phases caused by Ag addition and its refining effect on the primary Fe-rich phases and Cu grains. The inherent influence mechanism of this microstructure evolution on the improvement of the mechanical/electrical properties of Cu–Fe alloys has not been discussed deeply. Moreover, the magnetic performance optimization caused by adding Ag in Cu–Fe alloys has been rarely reported. In this study, the effect of accelerated Fe precipitation induced by Ag addition on the microstructure, electrical conductivity, mechanical properties, and magnetic properties of the as-cast, cold-rolled, and aged Cu–10Fe alloys was systematically investigated. The underlying mechanisms were carefully characterized and modeled.

II. EXPERIMENTAL DETAIL

A. Materials and Fabrication

Cu–10 wt pct Fe– x Ag alloys ($x = 0, 0.3, 1, 3,$ and 6 wt pct, actual component) with a diameter of 30 mm were prepared by electromagnetic continuous casting. The initial billets were cold-rolled with a total deformation of 90 pct and subsequently aged for 2 hours at 250 °C, 350 °C, 450 °C, and 500 °C to investigate the effect of Ag addition on the microstructure and comprehensive properties of Cu–10Fe alloys.

B. Microstructure Observation

The solidified microstructure of as-cast alloys was detected using an optical microscope (Keyence VW-9000) and a scanning electron microscope (SEM, TESCAN VEGA 3 Easy Probe). The average grain size was measured by using the centroidal method, *i.e.*, the mean length of the grain was obtained at two-degree intervals when passing through the grain's centroid.^[27] Image Pro software was used to determine the size (mean diameter) and volume fraction of Fe-rich precipitates.^[28] The samples were mechanically polished and then etched to expose the solidification microstructure. The microstructure parallel to the rolling direction was characterized using a JEOL JEM-2100F transmission electron microscope (TEM) at 200 kV. The samples were mechanically thinned to 50 μm and then ion-beam thinned for TEM observation. X-ray diffraction (XRD) measurements were conducted using a Bruker AXS D8 Advance diffractometer LynxEye detector.

C. Electrical, Magnetic, and Mechanical Testing

The electrical conductivities of Cu–Fe and Cu–Fe–Ag alloys were measured at room temperature by an RTS-11 four-probe resistivity tester.^[29–31] The saturation magnetization and coercivity were measured using a vibrating sample magnetometer (VSM, LakeShore 7400-S) with a maximum applied magnetic field of 1 T. The microhardness was tested using a Vickers hardness tester at HV0.2 (200gf) load with a dwell time of 10 seconds. Tensile tests were conducted at an initial strain rate of $3.5 \times 10^{-4} \text{ s}^{-1}$ at room temperature using an MTS tensile testing machine. Dogbone-shaped tensile samples with a cross section of $3.5 \times 1 \text{ mm}^2$ and a gauge length of 14 mm were cut parallel to the rolling direction using an electrical discharge machine. The strain was monitored by a 10-mm extensometer. All tests were performed three times to ensure reproducibility.

III. RESULTS AND DISCUSSION

A. Solidified Microstructure, Comprehensive Properties of As-cast Cu–Fe Alloys

Figure 1 displays that the grain refinement of as-cast Cu–Fe alloys is obtained by the addition of Ag. As the added Ag increases to 6 wt pct, the average grain size of the Cu matrix gradually drops from 110 to 29 μm (shown in Figure 1(f)). With the increase of the added Ag, the tensile properties of as-cast Cu–Fe alloys increase gradually (see electronic supplementary Figure S1). The morphology of primary Fe-rich spheres and dendrites was characterized and shown in Figure 2. Both the diameters of Fe-rich spheres and dendrite arms decrease monotonically with increasing added Ag, as shown in Figure 2(f). This is mainly because the added Ag can significantly reduce the interfacial energy between Cu and Fe, which in turn accelerates the precipitation of Fe, and finally promotes the simultaneous refinement of the Cu grains^[32–34] and primary micron-sized Fe-rich spheres/dendrites.^[35]

In addition, the Ag addition has a positive effect on the primary nano-sized Fe-rich precipitates in as-cast Cu–10Fe alloys. The size and distribution of nano-sized Fe-rich precipitates were carefully characterized by TEM, as shown in Figures 3(a) through (c). After adding 3 wt pct Ag, the average size of nano-sized Fe-rich precipitates decreases from 57.35 to 49.18 nm, while the volume fraction increases from 1.96 to 3.14 pct (shown in Figures 3(e) and (f)), indicating that the precipitation of nano-sized Fe-rich phases can be accelerated by the added Ag.

The magnetic properties of Cu–Fe alloys are affected by the precipitation of primary Fe-rich phases produced during solidification.^[36] Figure 3(h) shows that the magnetic properties of Cu–10Fe alloys gradually increase with increasing added Ag. This improvement of magnetic properties is related to the accelerated precipitation of primary micron-sized Fe-rich phases, which can be found in References 37–39, but whether the nano-sized Fe-rich precipitates play the same role

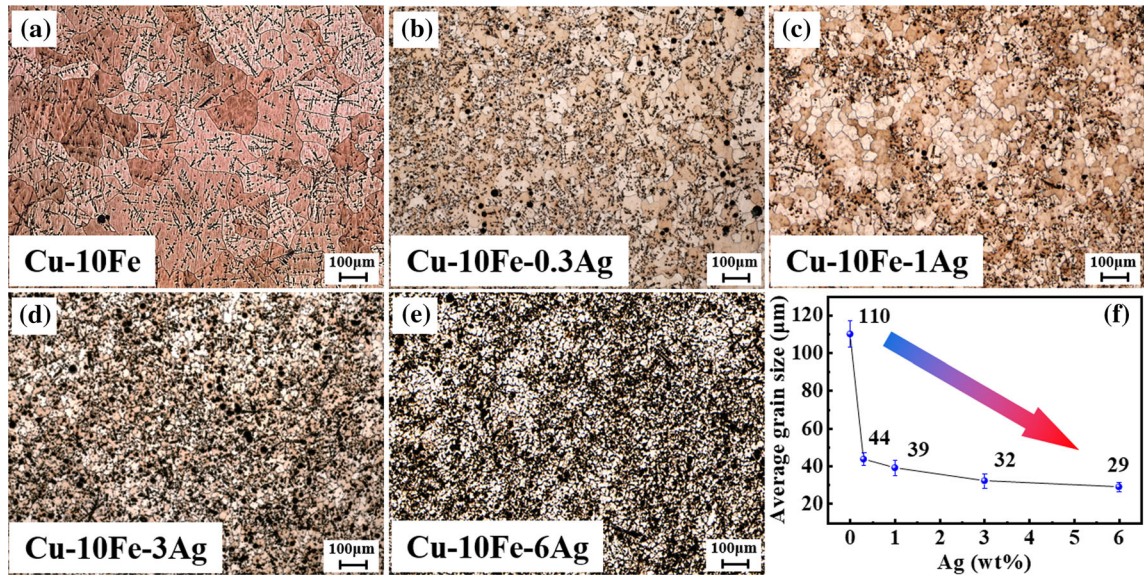


Fig. 1—Effect of added Ag on the grain refinement of as-cast Cu-10Fe alloys. (a) Cu-10Fe alloy, (b) Cu-10Fe-0.3Ag alloy, (c) Cu-10Fe-1Ag alloy, (d) Cu-10Fe-3Ag alloy, (e) Cu-10Fe-6Ag alloy, and (f) Effect of Ag addition on the average grain size of the Cu matrix.

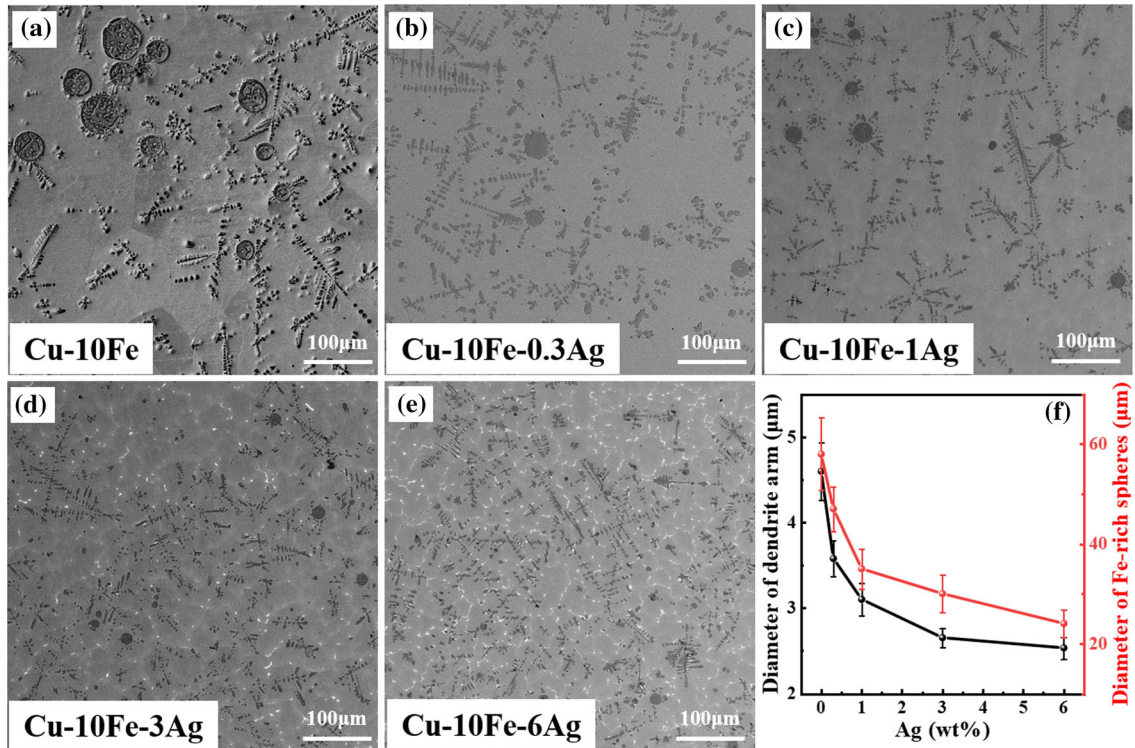


Fig. 2—Effect of added Ag on the refinement of primary micron-sized Fe-rich spheres/dendrites in as-cast Cu-10Fe alloys. (a) Cu-10Fe alloy, (b) Cu-10Fe-0.3Ag alloy, (c) Cu-10Fe-1Ag alloy, (d) Cu-10Fe-3Ag alloy, (e) Cu-10Fe-6Ag alloy, and (f) Effect of Ag addition on the diameters of Fe-rich spheres and dendrite arms.

has not been verified. Thus, to reveal the effect of nano-sized Fe-rich precipitates on the magnetic properties, the 0.08 wt pct Zr was added to the Cu-10Fe-3Ag alloy. Figure 3(i) shows that the saturation

magnetization of Cu-10Fe-3Ag alloy is greatly improved by Zr addition. However, the Zr addition does not have a significant effect on the size and volume fraction of nano-sized Fe-rich precipitates (shown in

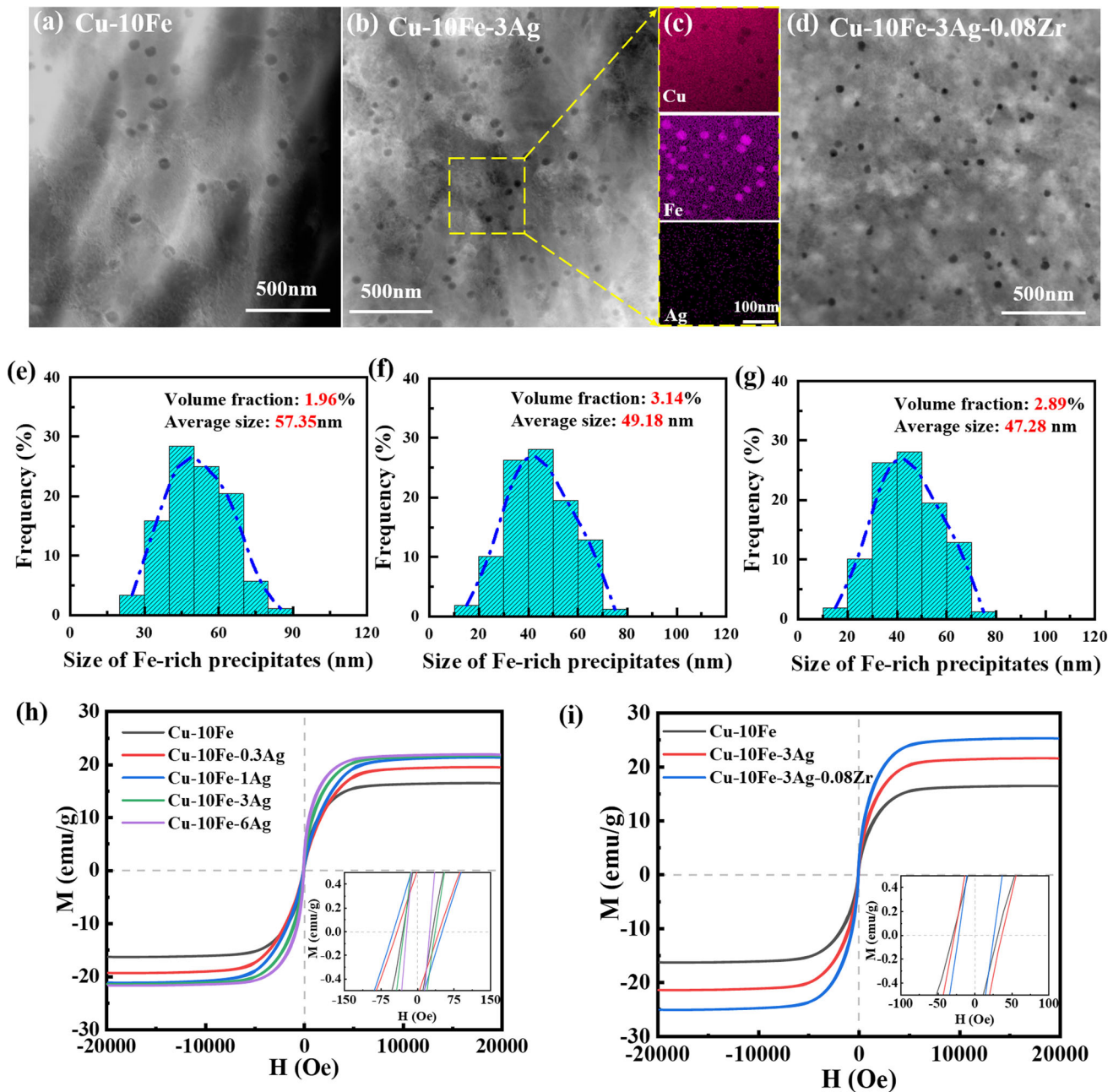


Fig. 3—Effects of Ag and Zr addition on the nano-sized Fe-rich precipitates and magnetic properties of as-cast Cu-10Fe alloys. (a), (b) and (d) Size and morphology of nano-sized Fe-rich precipitates in as-cast Cu-10Fe, Cu-10Fe-3Ag, and Cu-10Fe-3Ag-0.08Zr alloys, (c) Compositional mapping of the characteristic area (in the yellow box) in (b), (e) through (g) Size statistics of nano-sized Fe-rich precipitates in Cu-10Fe, Cu-10Fe-3Ag, and Cu-10Fe-3Ag-0.08Zr alloys, and (h) and (i) Effects of Ag and Zr addition on the magnetic properties of as-cast Cu-10Fe alloys (Color figure online).

Figures 3(d) and (g). Thus, it can be inferred that the improvement of magnetic properties comes from the contribution of primary micron-sized Fe-rich phases rather than that of nano-sized ones. Moreover, the evolution of micron-sized Fe-rich phases in as-cast Cu-10Fe alloys after Ag and Zr addition was calculated and shown in Figure 4. The saturation magnetization gradually increases with the increasing area fraction of micron-sized Fe-rich phases in the Cu matrix, which also

proves that the enhancement in magnetic properties is mainly dominated by the micron-sized Fe-rich spheres and dendrites.

The added Ag can be solid-dissolved into the Cu lattice, which will inevitably promote the precipitation of Fe, and then affect the electrical conductivity and microhardness of Cu-10Fe alloys. The electrical conductivity of as-cast Cu-10Fe alloys shows a monotonically increasing trend with increasing added Ag

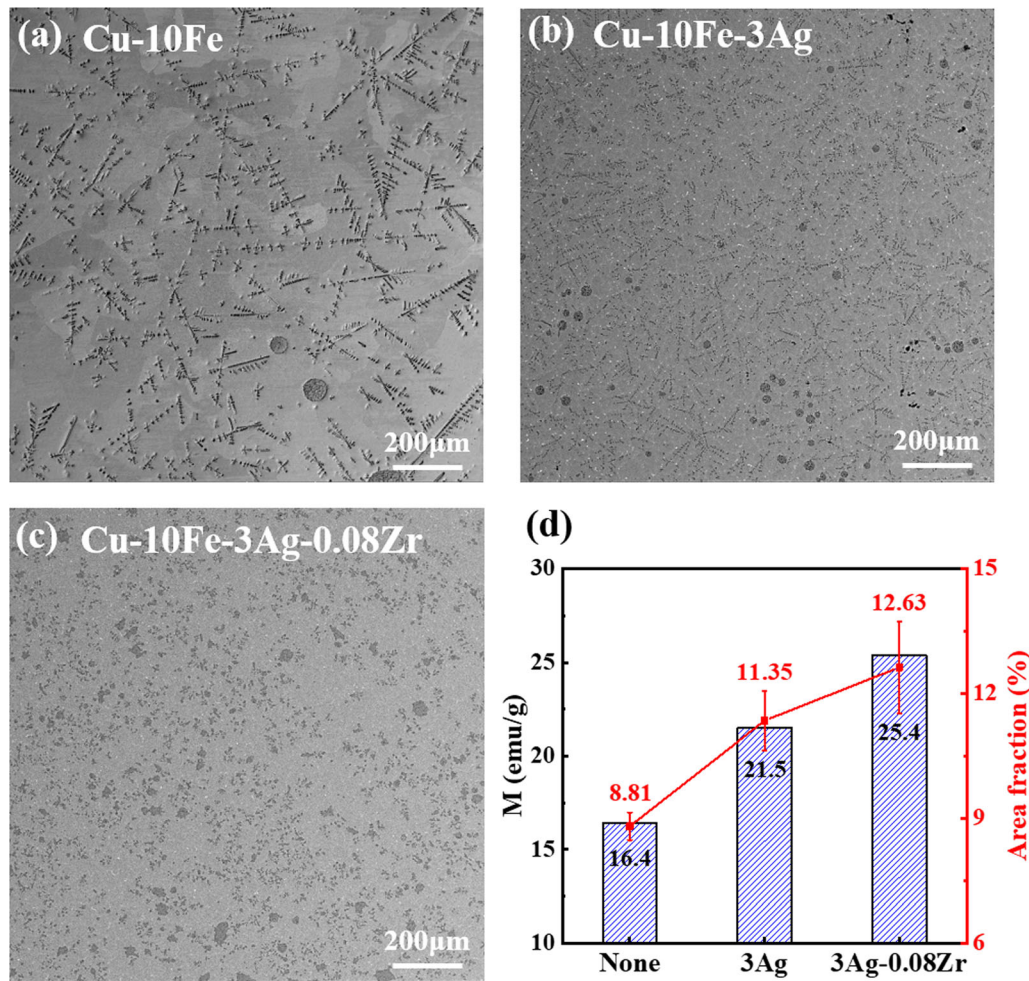


Fig. 4—Effects of Ag and Zr addition on the primary micron-sized Fe-rich phases. (a) through (c) SEM micrographs of micron-sized Fe-rich spheres and dendrites, and (d) Relationship between saturation magnetization and area fraction of micron-sized Fe-rich precipitates.

(Figure 5(a)). The solid solution of dissimilar elements in pure Cu, even the Ag element with the highest electrical conductivity in the world, will naturally lead to a drop in electrical conductivity.^[40] This abnormal increase in electrical conductivity caused by Ag addition has attracted our attention. Figures 5(a) and (b) shows that the content of Fe in the Cu matrix decreases while the microhardness gradually increases with increasing added Ag, which indicates that the added Ag takes the place of Fe in the Cu lattice. The lattice scattering caused by the solid solution of Ag is lower than that caused by the solid solution of Fe,^[22–24] which is the reason for the abnormal rise in the electrical conductivity of Cu–10Fe alloys induced by Ag addition. The atomic size difference between Ag and Cu is larger than that between Fe and Cu, so the solid solution strengthening brought by the Ag atom is higher than that brought by the Fe atom, which is the reason that the microhardness shows an upward trend as the Ag addition increases. This substitutional solid solution in as-cast Cu–Fe–Ag alloys was also verified by XRD and shown in Figures 5(c) and (d). The Cu (220) peak

gradually shifts to the lower angle as the Ag addition increases, indicating that the lattice constant of the Cu matrix increases according to Bragg's formula.^[41] The atomic radius of Ag, Cu, and Fe decreases in order, so the substitutional solid solution caused by Ag addition will lead to an increase in the lattice constant of the Cu matrix, which is consistent with the XRD results.

B. Strengthening Mechanism of Cold-Rolled Cu–Fe Alloys

Figures 6(a) displays that the yield strength of cold-rolled Cu–10Fe alloys increases monotonically with the increase of added Ag. The yield strength of Cu–10Fe–3Ag alloy is about 113 MPa higher than that of Cu–10Fe alloy. This improvement induced by Ag addition mainly results from the changes in solid solution strengthening (σ_{SS}), dislocation strengthening (σ_D), precipitation strengthening (σ_P), and grain refinement strengthening (σ_{GB}). Table I shows all the parameters used to calculate these different strengthening contributions.

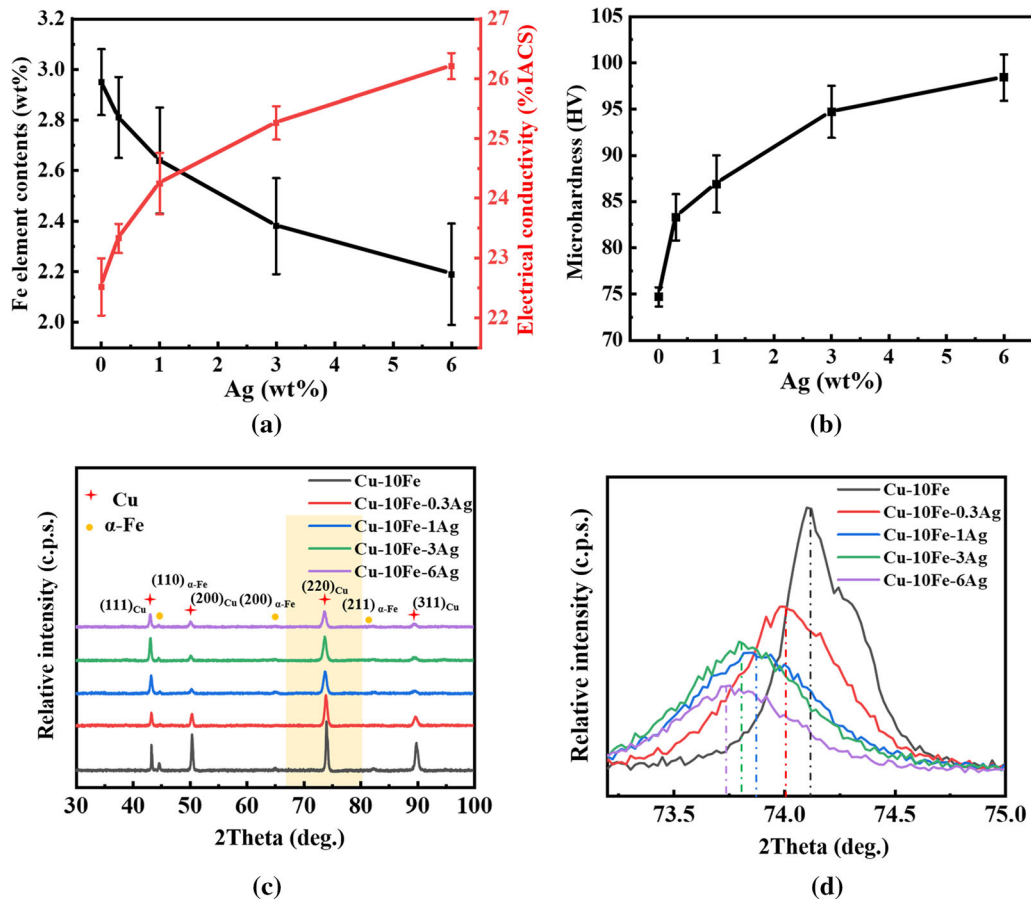


Fig. 5—Effect of Ag addition on Fe content in the Cu matrix and the electrical conductivity, microhardness, and XRD patterns of Cu-10Fe alloys. (a) Fe content in the Cu matrix and electrical conductivity of Cu-10Fe alloys, (b) Microhardness, (c) XRD full patterns, and (d) Peaks of Cu (220) crystal planes.

1. Precipitation strengthening

The difference between the Cu-10Fe and Cu-10Fe-3Ag alloys in precipitation strengthening is given below^[42]:

$$\Delta\sigma_P = \frac{0.81MGb}{2\pi(1-\nu)^{1/2}} \frac{\ln(2r/b)}{\lambda - 2r} \quad [1]$$

$$\lambda = r \left(\frac{3\pi}{2f_v} \right)^{1/2} \quad [2]$$

where M is the Taylor factor, G is the shear modulus of the Cu matrix, b is the Burgers vector of the Cu matrix, ν is the Poisson ratio, r and f_v are the average radius and volume fraction of the Fe-rich precipitates, and λ is the average crystal plane spacing between Fe-rich precipitates, which can be estimated by using Eq. [2]. The nano-sized Fe-rich precipitates observed by TEM in the solidified microstructure do not change significantly during the cold-rolling process. Therefore, the average radius r and volume fraction f_v of the Fe-rich precipitates in Cu-10Fe and Cu-10Fe-3Ag alloys are, respectively, set as 28.68 nm, 1.96 pct, and 24.59 nm, 3.14 pct.

The strengthening contribution due to the nano-sized Fe-rich precipitates is calculated as 80.3 and 119.6 MPa for the cold-rolled Cu-10Fe and Cu-10Fe-3Ag alloys, respectively. Therefore, the difference in precipitation strengthening $\Delta\sigma_P$ caused by Ag addition is 39.3 MPa.

2. Dislocation strengthening

Figures 6(c) through (e) shows lots of dislocation tangles around the nano-size Fe-rich precipitates, which is caused by the severe pinning effect of Fe-rich precipitates on the dislocation movement during cold-rolling. The accelerated nano-sized Fe-rich precipitation can be induced by the Ag addition; thus, it has a higher dislocation density in cold-rolled Cu-10Fe-3Ag alloy. The dislocation-induced strengthening can be calculated as follows^[43-45]:

$$\Delta\sigma_D = MG\alpha b\sqrt{\rho} \quad [3]$$

$$\rho = \frac{16.1 \times \varepsilon^2}{b^2} \quad [4]$$

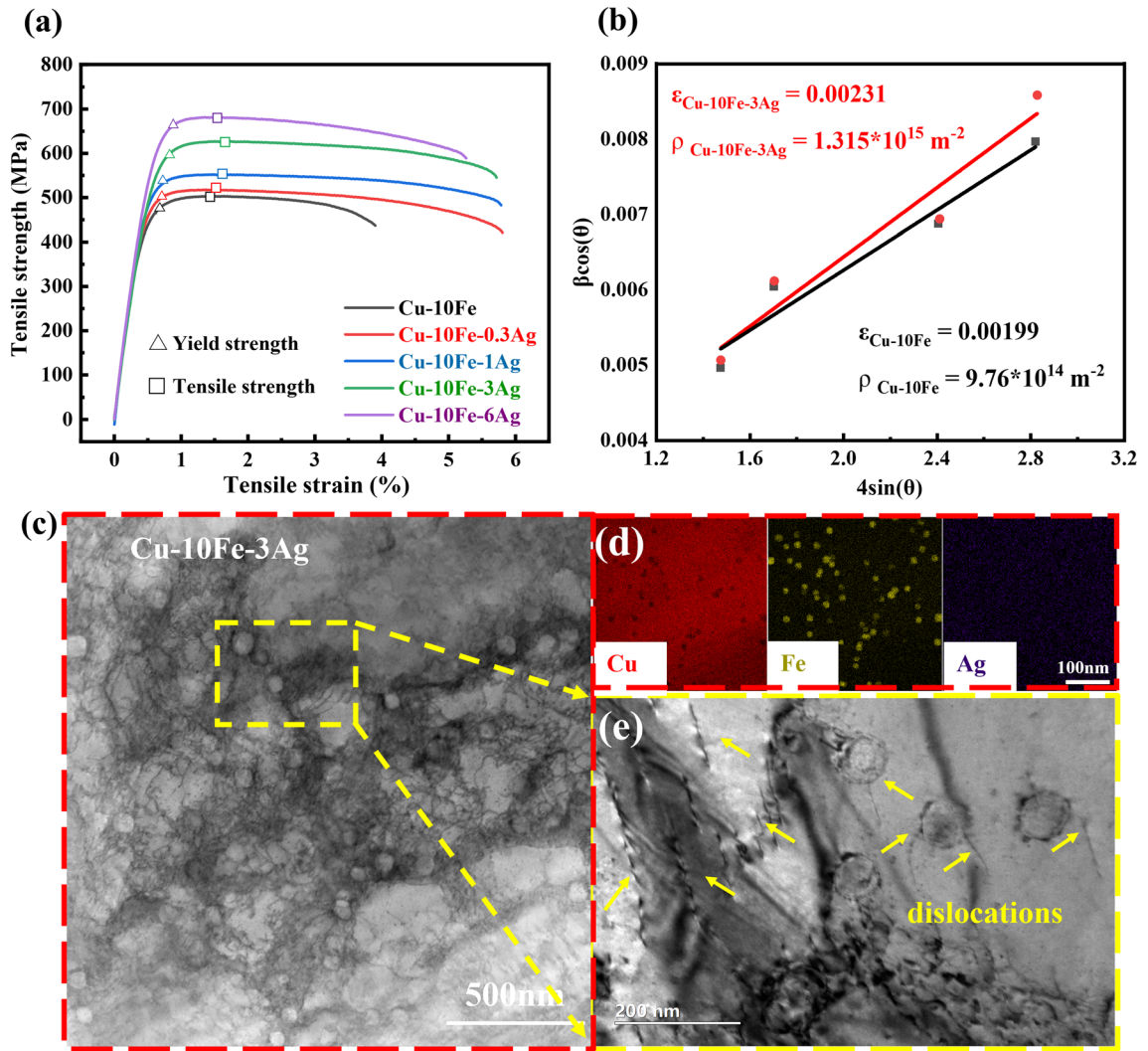


Fig. 6—Effect of Ag addition on the mechanical properties of cold-rolled Cu-10Fe alloys. (a) Stress-strain curves, (b) statistics of dislocation density and microstrain in Cu-10Fe and Cu-10Fe-3Ag alloys, (c) microstructure of cold-rolled Cu-10Fe-3Ag alloy characterized by TEM, (d) compositional mapping for (c) (in the red box), showing that Ag is uniformly distributed in the Cu matrix and no new precipitates are formed, and (e) enlarge view of the dislocations around the nano-sized Fe-rich precipitates (in the yellow box) (Color figure online).

Table I. Parameters Used in the Calculation of Strengthening Contributions

Parameter	Description	Value	Units	References
M	Taylor factor	3.06	—	[47]
G	shear modulus of Cu matrix	46	GPa	[48]
b	burgers vector of Cu matrix	0.2556	nm	[49]
ν	Poisson ratio	0.34	—	[50]
α	a constant	0.2	—	[51]

$$\beta \cos \theta = \frac{K\lambda}{D} + (4 \sin \theta) \cdot \varepsilon \quad [5]$$

where α is a constant, ρ is the dislocation density, β is the half-peak width of Cu peaks in XRD patterns, θ is the

Bragg angle of a certain peak, and ε is the microstrain which can be obtained by linear fitting of $4 \sin(\theta)$ and $\beta \cos(\theta)$ according to Eq. [5] based on Hall-Williamson's method.^[46] The microstrain and dislocation density in Cu-10Fe and Cu-10Fe-3Ag were calculated and shown

in Figure 6(b). Thus, the strengthening contribution due to the dislocation can be estimated as 220.3 and 262.6 MPa for the cold-rolled Cu–10Fe and Cu–10Fe–3Ag alloys, respectively. The difference in

dislocation strengthening $\Delta\sigma_D$ caused by Ag addition is 42.3 MPa.

The strengthening contribution due to the solid solution and grain refinement can be estimated as 169.4 and 200.8 MPa for the cold-rolled Cu–10Fe and

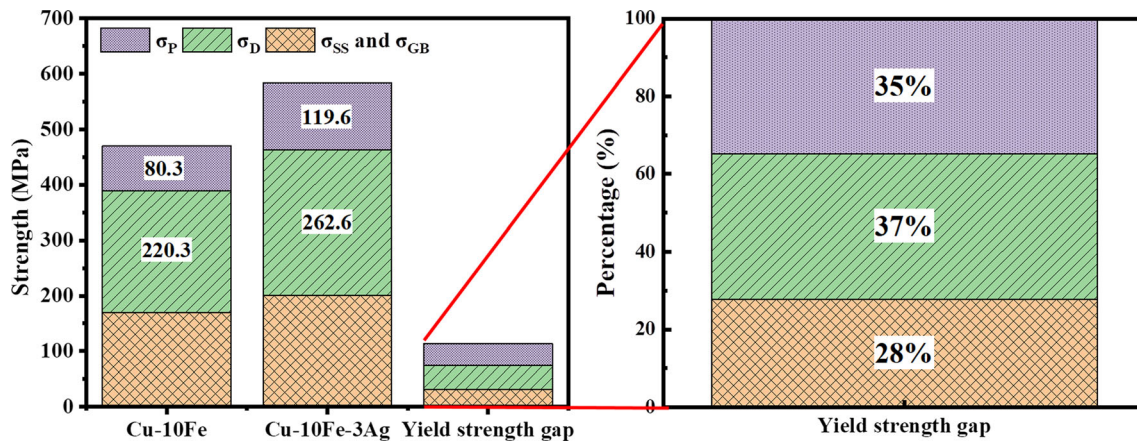


Fig. 7—Quantification of strengthening contributions.

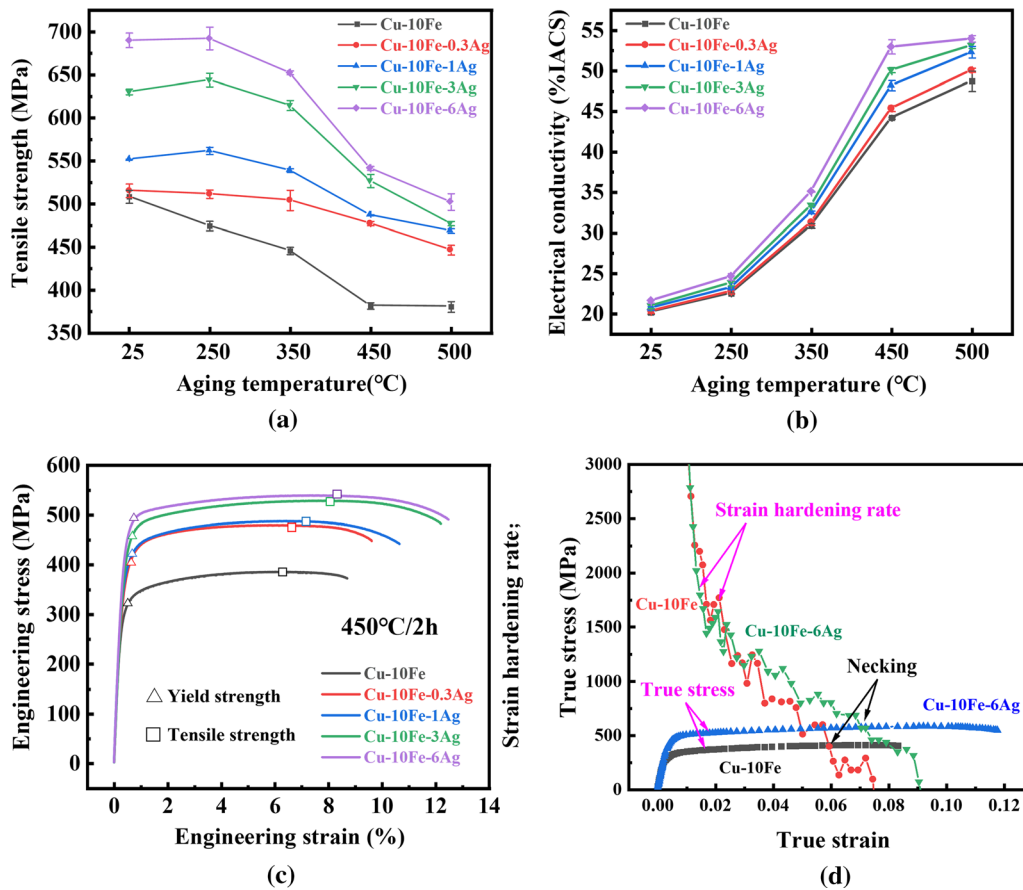


Fig. 8—Effect of Ag addition on the mechanical properties and electrical conductivity of aged Cu–10Fe alloys. (a) Tensile strength, (b) electrical conductivity, (c) engineering stress–strain curves of Cu–10Fe and Cu–10Fe–Ag alloys, and (d) Strain hardening curves of Cu–10Fe and Cu–10Fe–6Ag alloys.

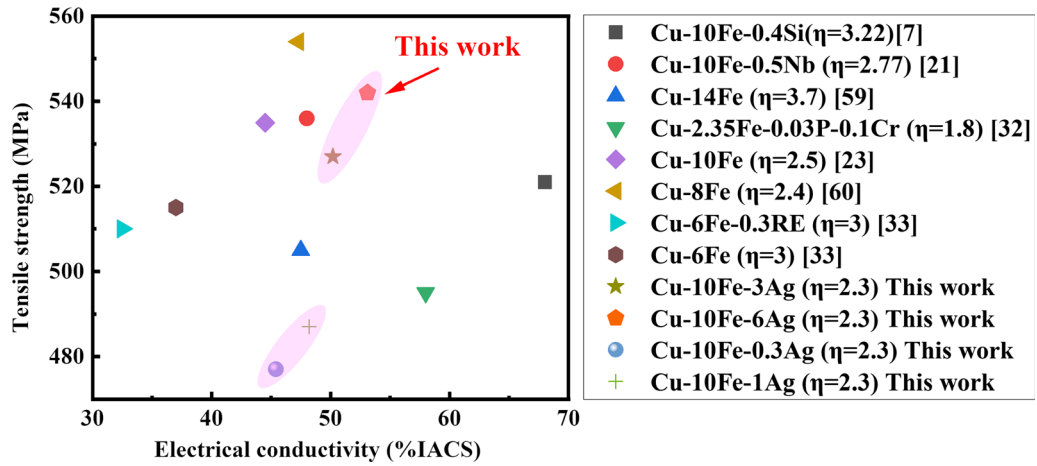


Fig. 9—Tensile strength versus electrical conductivity of different Cu–Fe alloys under similar deformation strains in comparison with available literature data^[7,21,23,32,33,59,60].

Cu–10Fe–3Ag alloys, respectively. The total difference in solid solution strengthening and grain refinement strengthening induced by Ag addition is 31.4 MPa. These four strengthening contributions were counted and shown in Figure 7. The strengthening contributions in the cold-rolled Cu–10Fe and Cu–10Fe–3Ag alloys are dominated by precipitation strengthening and dislocation strengthening. Moreover, the difference in yield strength between the cold-rolled Cu–10Fe and Cu–10Fe–3Ag results from the accelerated precipitation of nano-sized Fe-rich phases and their pinning effect on dislocation movement.

C. Strength–Ductility–Electrical Conductivity Synergy in Aged Cu–Fe Alloys

The synergistic improvement of strength, ductility and electrical conductivity of Cu alloys can be obtained by tailoring appropriate aging temperature.^[52,53] The effect of aging temperature on the strength and electrical conductivity of Cu–10Fe and Cu–10Fe–Ag alloys was measured, as shown in Figure 8. With the increase in aging temperature, the tensile strength of Cu–10Fe–Ag alloys shows a downward trend, while the electrical conductivity gradually increases. The Cu–10Fe–6Ag alloy obtains an optimal comprehensive performance after being aged for 2 hours at 450 °C, where the yield strength, tensile strength, uniform elongation, and electrical conductivity reach 484.2 MPa, 539.1 MPa, 7.9 and 53 pct IACS, respectively.

It can be found that the added Ag enables the Cu–10Fe alloy to obtain a better match of strength and ductility, as shown in Figure 8(c). To investigate the underlying mechanism of ductility improvement, the strain hardening rate θ ^[54] ($\theta = d\sigma/d\varepsilon$, where σ and ε are true stress and true strain, respectively) vs. true strain curve of Cu–10Fe and Cu–10Fe–6Ag alloys was calculated and shown in Figure 8(d). A higher strain hardening capacity is obtained by adding Ag to the Cu–10Fe alloy, thereby delaying the onset of necking according to

the Considère criterion and breaking the strength–ductility trade-off.^[55–57] A summary of tensile strength and electrical conductivity of the reported Cu–Fe alloys under similar deformation strains is displayed in Figure 9. The deformation strain can be set as $\eta = \ln(A_0/A_f)$,^[58] where A_0 and A_f are the cross-sectional areas of the samples before and after deformation, respectively. It can be seen that a better synergistic improvement effect can be obtained by adding Ag to Cu–Fe alloys.

IV. CONCLUSION

In this study, the effect of Ag addition on the solidified microstructure and comprehensive properties of Cu–10Fe alloys was systematically investigated. The main conclusions can be summarized as follows:

- (1) The precipitation of Fe can be accelerated by the added Ag, which in turn induces the simultaneous refinement of Cu grains, micron-sized primary Fe-rich spheres and dendrites, and nano-sized Fe-rich precipitates in the solidified microstructure of as-cast Cu–10Fe alloys.
- (2) The saturation magnetization of Cu–10Fe alloys is improved from 16.4 to 21.5 emu/g by adding 3 wt pct Ag. Results show that the improvement of magnetic properties is dominated by the accelerated precipitation of micron-sized Fe-rich spheres and dendrites, rather than that of nano-sized Fe-rich precipitates.
- (3) The yield strength of cold-rolled Cu–10Fe alloys is improved from 465.1 to 591.8 MPa by adding 3 wt pct Ag, which is mainly attributed to the accelerated precipitation of nano-sized Fe-rich phases and their pinning effect on dislocation movement during cold-rolling.
- (4) Optimal comprehensive performance of Cu–10Fe–6Ag alloy is obtained after being aged

for 2 hours at 450 °C, where the yield strength, tensile strength, uniform elongation and electrical conductivity reach 484.2, 539.1 MPa, 7.9 and 53 pct IACS, respectively.

ACKNOWLEDGMENTS

The present research was supported by the National Natural Science Foundation of China [Grant Numbers 51904184, U1860202, U1732276, 50134010, 52004156], Independent Research and Development Project of State Key Laboratory of Advanced Special Steel, Shanghai Key Laboratory of Advanced Ferrometallurgy, Shanghai University (SKLASS 2021-Z10 and 11), and Science and Technology Commission of Shanghai Municipality [Grant Numbers 13JC14025000, 15520711000, 19DZ2270200, 20511107700]. We sincerely thank Jianchao Peng and Na Min for their help with the TEM testing at Shanghai University.

CONFLICT OF INTEREST

The authors declare that they have no known competing financial interests or personal relationships that could have appeared to influence the work reported in this manuscript.

SUPPLEMENTARY INFORMATION

The online version contains supplementary material available at <https://doi.org/10.1007/s11661-022-06927-4>.

REFERENCES

1. Z. Shen, Z.Z. Lin, P.J. Shi, J.L. Zhu, T.X. Zheng, B. Ding, Y.F. Guo, and Y.B. Zhong: *J. Mater. Sci. Technol.*, 2022, vol. 110, pp. 187–97.
2. Z. Shen, Z.Z. Lin, P.J. Shi, G.P. Tang, T.X. Zheng, C.M. Liu, Y.F. Guo, and Y.B. Zhong: *Mater. Sci. Eng. A*, 2021, vol. 820, p. 141548.
3. W.Y. Li, X.P. Guo, C. Verdy, L. Dembinski, H.L. Liao, and C. Coddet: *Scr. Mater.*, 2006, vol. 55, pp. 327–30.
4. C. Zhao, Z. Wang, D.X. Li, L. Kollo, Z.Q. Luo, W.W. Zhang, and K.G. Prashanth: *Int. J. Plast.*, 2021, vol. 138, p. 102926.
5. W.J. Liu, X. Chen, T. Ahmad, C.Y. Zhou, X.P. Xiao, H. Wang, and B. Yang: *Mater. Sci. Eng. A*, 2022, vol. 835, p. 142672.
6. X. Luo, D.W. Yuan, H. Wang, H.M. Chen, X.P. Xiao, B.J. Han, H. Huang, and B. Yang: *J. Magn. Magn. Mater.*, 2022, vol. 556, p. 169407.
7. Y.J. Pang, G.H. Chao, T.Y. Luan, S. Gong, Y.R. Wang, Z.H. Jiang, Z. Xiao, Y.B. Jiang, and Z. Li: *Mater. Sci. Eng. A*, 2021, vol. 826, p. 142012.
8. D.W. Yuan, X.P. Xiao, X. Luo, H. Wang, B.J. Han, B.X. Liu, and B. Yang: *Mater. Charact.*, 2022, vol. 185, p. 111707.
9. J.D. Verhoeven, S.C. Chueh, and E. Gibson: *J. Mater. Sci.*, 1989, vol. 24, pp. 1748–52.
10. S.C. Liu, J.C. Jie, Z.K. Guo, S.P. Yue, and T.J. Li: *Mater. Chem. Phys.*, 2019, vol. 238, p. 121909.
11. M. Wang, Y.B. Jiang, Z. Li, Z. Xiao, S. Gong, W.T. Qiu, and Q. Lei: *Mater. Sci. Eng. A*, 2021, vol. 801, p. 140379.
12. S.C. Liu, S.S. Xu, J.C. Jie, J.J. Zhang, Y. Dong, X.Z. Li, and T.J. Li: *J. Alloy. Compd.*, 2021, vol. 888, p. 161627.
13. C. Biselli and D.G. Morris: *Acta Mater.*, 1996, vol. 44, pp. 493–504.
14. X. Sauvage, F. Wetscher, and P. Pareige: *Acta Mater.*, 2005, vol. 53, pp. 2127–35.
15. Z.W. Wu, J.D. Zhang, Y. Chen, and L. Meng: *J. Rare Earths*, 2009, vol. 27, pp. 87–91.
16. L. Ren, S.S. Zhang, J.Q. Shi, Z. Shen, P.J. Shi, T.X. Zheng, B. Ding, Y.F. Guo, Q.L. Xiao, Q. Li, and Y.B. Zhong: *Mater. Sci. Eng. A*, 2022, vol. 846, p. 143309.
17. Z.F. Han, G.L. Xie, X.H. Liu, Q. Tan, and R. Wang: *J. Mater. Sci. Technol.*, 2022, vol. 98, pp. 1–3.
18. D.H. Kim and K.H. Lee: *Kor. J. Mater. Res.*, 2010, vol. 20, pp. 60–64.
19. Y.B. Jeong, H.R. Jo, J.T. Kim, S.H. Hong, and K.B. Kim: *J. Alloy. Compd.*, 2019, vol. 786, pp. 341–45.
20. S. Sarkar, C. Srivastava, and K. Chattopadhyay: *Mater. Sci. Eng. A*, 2018, vol. 723, pp. 38–47.
21. P. Zhang, Q. Lei, X.B. Yuan, X.F. Sheng, D. Jiang, Y.P. Li, and Z. Li: *Mater. Today Commun.*, 2020, vol. 25, p. 101353.
22. H.Y. Gao, J. Wang, D. Shu, and B.D. Sun: *Scr. Mater.*, 2005, vol. 53, pp. 1105–09.
23. Y. Li, D.Q. Yi, and J.B. Zhang: *J. Alloy. Compd.*, 2015, vol. 647, pp. 413–18.
24. Z.X. Xie, H.Y. Gao, Q. Lu, J. Wang, and B.D. Sun: *J. Alloy. Compd.*, 2010, vol. 508, pp. 320–23.
25. Y.F. Wang, H.Y. Gao, J. Wang, Y.F. Han, Y.B. Dai, and B.D. Sun: *Solid State Commun.*, 2014, vol. 183, pp. 60–63.
26. D.W. Yuan, X.P. Xiao, J.S. Chen, B.J. Han, H. Huang, and B. Yang: *J. Alloy. Compd.*, 2021, vol. 887, p. 161458.
27. Z. Shen, B.F. Zhou, J. Zhong, Y.B. Zhong, T.X. Zheng, L.C. Dong, Y. Zhai, W.L. Ren, Z.S. Lei, and Z.M. Ren: *Metall. Mater. Trans. B*, 2019, vol. 50B, pp. 2111–20.
28. F. Zhang, J.Y. He, Y. Wu, H.H. Mao, H. Wang, X.J. Liu, S.H. Jiang, T.G. Nieh, and Z.P. Lu: *Mater. Sci. Eng. A*, 2022, vol. 839, p. 142879.
29. C.H. Lei, H.Y. Yang, F. Zhao, X.Y. Fang, Y.T. Fang, L. Meng, J.B. Liu, and H.T. Wang: *J. Mater. Sci.*, 2021, vol. 56, pp. 14821–31.
30. H.Y. Yang, Y.Q. Bu, J.M. Wu, Y.T. Fang, J.B. Liu, H.T. Wang, and W. Yang: *Mater. Charact.*, 2021, vol. 176, p. 111099.
31. H.Y. Yang, K.Q. Li, Y.Q. Bu, J.M. Wu, Y.T. Fang, L. Meng, J.B. Liu, and H.T. Wang: *Scr. Mater.*, 2021, vol. 195, p. 113741.
32. F.A. Guo, C.J. Xiang, C.X. Yang, X.M. Cao, S.G. Mu, and Y.Q. Tang: *Mater. Sci. Eng. B*, 2008, vol. 147, pp. 1–6.
33. Z.W. Wu, Y. Chen, and L. Meng: *J. Alloy. Compd.*, 2009, vol. 477, pp. 198–204.
34. W. Chen, X.N. Hu, W. Guo, J. Zou, K. Liu, D.P. Lu, and D.Q. Tan: *Mater.*, 2019, vol. 12, p. 2772.
35. P. Zhang, X.B. Yuan, Y.D. Li, Y.H. Zhou, R.L. Lai, Y.P. Li, Q. Lei, and A. Chiba: *J. Alloy. Compd.*, 2022, vol. 904, p. 163983.
36. K. Sumiyama, T. Yoshitake, and Y. Nakamura: *J. Phys. Soc. Jpn.*, 1984, vol. 53, pp. 3160–65.
37. C.L. Chien, S.H. Liou, D. Kofalt, W. Yu, T. Egami, and T.R. McGuire: *Phys. Rev. B*, 1986, vol. 33, pp. 3247–50.
38. E. Ma, M. Atzmon, and F. Pinkerton: *J. Appl. Phys.*, 1993, vol. 74, pp. 955–62.
39. C.Z. Zhang, C.G. Chen, L.N. Huang, T.X. Lu, P. Li, W.W. Wang, F. Zhang, A.A. Volinsky, and Z.M. Guo: *Powder Metall.*, 2021, vol. 64, pp. 308–20.
40. Y. Sakai and H.J. Schneider-Muntau: *Acta Mater.*, 1997, vol. 45, pp. 1017–23.
41. S.Q. Xi, K.S. Zuo, X.G. Li, G. Ran, and J.G. Zhou: *Acta Mater.*, 2008, vol. 56, pp. 6050–60.
42. J.Z. Li, H. Ding, B.M. Li, W.L. Gao, J. Bai, and G. Sha: *Mater. Sci. Eng. A*, 2021, vol. 802, p. 140628.
43. H.T. Jeong and W.J. Kim: *J. Mater. Sci. Technol.*, 2021, vol. 71, pp. 228–40.

44. Y.J. Ban, Y.F. Geng, J.R. Hou, Y. Zhang, M. Zhou, Y.L. Jia, B.H. Tian, Y. Liu, X. Li, and A.A. Volinsky: *J. Mater. Sci. Technol.*, 2021, vol. 93, pp. 1–6.
45. J.K. Li, T. Cheng, Y.B. Liu, Y.Q. Yang, W. Li, and Q.S. Wei: *Addit. Manuf.*, 2022, vol. 54, p. 102726.
46. F. HajyAkbar, J. Sietsma, A.J. Böttger, and M.J. Santofimia: *Mater. Sci. Eng. A*, 2015, vol. 639, pp. 208–18.
47. Q. Lei, Z. Xiao, W.P. Hu, B. Derby, and Z. Li: *Mater. Sci. Eng. A*, 2017, vol. 697, pp. 37–47.
48. P.H.F. Oliveira, D.C.C. Magalhães, M.T. Izumi, O.M. Cintho, A.M. Kliauga, and V.L. Sordi: *Mater. Sci. Eng. A*, 2021, vol. 813, p. 141154.
49. J.S. Chen, J.F. Wang, X.P. Xiao, H. Wang, H.M. Chen, and B. Yang: *Mater. Sci. Eng. A*, 2019, vol. 756, pp. 464–73.
50. G.M. Zhang, S.C. Liu, C. Chen, X.Y. Zhang, X.P. Gan, Q. Lei, Z. Li, and K.C. Zhou: *Mater. Sci. Eng. A*, 2019, vol. 763, p. 138132.
51. Z.F. Hao, G.L. Xie, X.H. Liu, Q. Tan, and R. Wang: *J. Mater. Sci. Technol.*, 2022, vol. 98, pp. 1–3.
52. N.N. Liang, J.Z. Liu, S.C. Lin, Y. Wang, J.T. Wang, Y.H. Zhao, and Y.T. Zhu: *J. Alloy. Compd.*, 2018, vol. 735, pp. 1389–94.
53. G. Purcek, H. Yanar, M. Demirtas, Y. Alemdag, D. Shangina, and S.V. Dobatkin: *Mater. Sci. Eng. A*, 2016, vol. 649, pp. 114–22.
54. K. Ameyama, F. Cazes, H. Couque, G. Dirras, S. Kikuchi, J. Li, F. Mompiau, K. Mondal, D. Orlov, B. Sharma, D. Tingaud, and S.K. Vajpai: *Mater. Res. Lett.*, 2022, vol. 10, pp. 440–71.
55. Y.T. Zhu, K. Ameyama, P.M. Anderson, I.J. Beyerlein, H.J. Gao, H.S. Kim, E. Lavernia, S. Mathaudhu, H. Mughrabi, R.O. Ritchie, N. Tsuji, X.Y. Zhng, and X.L. Wu: *Mater. Res. Lett.*, 2021, vol. 9, pp. 1–31.
56. X.L. Wu, M.X. Yang, F.P. Yuan, G.L. Wu, Y.J. Wei, X.X. Huang, and Y.T. Zhu: *Proc. Natl. Acad. Sci.*, 2015, vol. 112, pp. 14501–05.
57. X.T. Fang, G.Z. He, C. Zheng, X.L. Ma, D. Kaoumi, Y.S. Li, and Y.T. Zhu: *Acta Mater.*, 2020, vol. 186, pp. 644–55.
58. M.A. Abdulstaar, E.A. El-Danaf, N.S. Waluyo, and L. Wagner: *Mater. Sci. Eng. A*, 2013, vol. 565, pp. 351–58.
59. J. Zou, D.P. Lu, Q.F. Fu, K.M. Liu, and J. Jiang: *Vacuum*, 2019, vol. 167, pp. 54–58.
60. Z.X. Xie, H.Y. Gao, S.J. Wang, J. Wang, H. Huang, and P. Luo: *Mater. Trans.*, 2013, vol. 54, pp. 2075–78.

Publisher’s Note Springer Nature remains neutral with regard to jurisdictional claims in published maps and institutional affiliations.

Springer Nature or its licensor (e.g. a society or other partner) holds exclusive rights to this article under a publishing agreement with the author(s) or other rightsholder(s); author self-archiving of the accepted manuscript version of this article is solely governed by the terms of such publishing agreement and applicable law.